Synthesis, Chirality, and Magnetic Properties of Bimetallic Cyanide-Bridged Two-Dimensional Ferromagnets

Eugenio Coronado,*[,†] Carlos J. Gómez-García,[†] Alicia Nuez,[†] Francisco M. Romero,*[,†] and João C. Waerenborgh[‡]

Instituto de Ciencia Molecular, Universitat de València, P.O. Box 22085, 46071 València, Spain, and Departamento de Química, Instituto Tecnológico e Nuclear, P-2686-953 Sacavém, Portugal

Received January 13, 2006. Revised Manuscript Received March 20, 2006

The assembly of hexacyanoferrate(III) anions and nickel(II) bis-diamino complexes of the chiral ligand *trans*-cyclohexane-1,2-diamine (*trans*-chxn) yields cyanide-bridged two-dimensional ferromagnets of the general formula $[Ni(\textit{trans}\text{-chxn})_2]_3[Fe(CN)_6]_2 \cdot 2H_2O$. Their crystal structure is built from cyanide-bridged bimetallic planes separated by the bulky chxn ligands, giving rise to a large interlayer distance ($d = 11.7$ Å). These materials order ferromagnetically at the Curie temperature $T_C = 14$ K. AC susceptibility measurements evidence an unusual magnetic behavior below T_C, with a marked frequency dependence. A thorough magnetic analysis demonstrates that this complex behavior is due to the pinning of the domain walls which results from the coexistence of the layered structure and the strong magnetic anisotropy. An activation energy for domain wall movement $E_a = 116$ K has been determined. Ferromagnetic materials of this kind that incorporate structural chirality have been obtained by using the enantiopure ligands *trans*-(1*S*,2*S*)-chxn and *trans*-(1*R*,2*R*)-chxn, as evidenced by circular dichroism spectroscopy. The ligand *cis*-cyclohexane-1,2-diamine affords also a two-dimensional compound of formula $[Ni(\textit{cis}\text{-chxn})_2]_3[Fe(CN)_6]_2 \cdot 2H_2O$. This material orders ferromagnetically at $T_C = 11$ K and also exhibits slow relaxation behavior.

Introduction

Prussian blue (PB), the first synthetic coordination compound reported in the scientific literature, and its analogues are currently under active investigation for their electronic applications (electrochromic displays, photoresponsive electrodes, batteries, electrocatalysis, biosensing, etc.).[1,2] In molecular magnetism, the renaissance of the PB family was driven by the observation of high magnetic ordering temperatures in these materials.[3−6] Archetypal room-temperature molecular magnets belong to this family.[7,8] Further, the coexistence of magnetic order and electron-transfer properties in PB derivatives makes them very attractive for the design of magnets that are sensitive to electronical perturbations induced by temperature,[9] light irradiation,[10−12] or applied pressure.[13,14] PB-like compounds are bimetallic cyanides that can be obtained by reaction of hexacyanometalate anions $[M(CN)_6]^{y-}$ with metal aquo complexes $[M'(H_2O)_n]^{x+}$. Under these conditions, the six cyanide anions behave as bridging bidentate ligands and a cubic perovskite-like structure results.[15] The stoichiometry of the resulting compounds $M'_y[M(CN)_6]_x$ is given by the metal oxidation states and by the presence of alkali metal cations in the interstices of the three-dimensional (3D) structure. When the stoichiometric ratio $y/x > 1$, a certain number of $[M(CN)_6]^{y-}$ vacancies appear.

Parallel to the magnetic study of PB-like phases, a new family of cyanide-bridged magnetic molecular compounds has been developed by reaction of hexacyanometalate anions with metal precursors of the type $[M'(L)_n(H_2O)_m]$ (L = diamine ligand).[16−23] Because L is a stronger ligand, this

* To whom correspondence should be addressed. E-mail: fmrm@uv.es. Phone: +34 963544405. Fax: +34 963543273.
† Universitat de València.
‡ Instituto Tecnológico e Nuclear.

(1) Itaya, K.; Uchida, I.; Neff, V. D. *Acc. Chem. Res.* **1986**, *19*, 162.
(2) de Tacconi, N. R.; Rajeshwar, K.; Lezna, R. O. *Chem. Mater.* **2003**, *15*, 3046.
(3) Gadet, V.; Mallah, T.; Castro, I.; Verdaguer, M.; Veillet, P. *J. Am. Chem. Soc.* **1992**, *114*, 9213.
(4) Mallah, T.; Thiébaut, S.; Verdaguer, M.; Veillet, P. *Science* **1993**, *262*, 1554.
(5) Entley, W. R.; Girolami, G. S. *Inorg. Chem.* **1994**, *33*, 5165.
(6) Entley, W. R.; Girolami, G. S. *Science* **1995**, *268*, 397.
(7) Ferlay, S.; Mallah, T.; Ouahès, R.; Veillet, P.; Verdaguer, M. *Nature* **1995**, *378*, 701.
(8) Garde, R.; Villain, F.; Verdaguer, M. *J. Am. Chem. Soc.* **2002**, *124*, 10531.
(9) Shimamoto, N.; Ohkoshi, S.; Sato, O.; Hashimoto, K. *Inorg. Chem.* **2002**, *41*, 678.
(10) Sato, O.; Iyoda, T.; Fujishima, A.; Hashimoto, K. *Science* **1996**, *272*, 704.
(11) Sato, O.; Einaga, Y.; Fujishima, A.; Hashimoto, K. *Inorg. Chem.* **1999**, *38*, 4405.
(12) Bleuzen, A.; Lomenech, C.; Escax, V.; Villain, F.; Varret, F.; Cartier dit Moulin, C.; Verdaguer, M. *J. Am. Chem. Soc.* **2000**, *122*, 6648.
(13) Ksenofontov, V.; Levchenko, G.; Reiman, S.; Gütlich, P.; Bleuzen, A.; Escax, V.; Verdaguer, M. *Phys. Rev. B* **2003**, *68*, 024415.
(14) Coronado, E.; Giménez-López, M. C.; Levchenko, G.; Romero, F. M.; García-Baonza, V.; Milner, A.; Paz-Pasternak, M. *J. Am. Chem. Soc.* **2005**, *127*, 4580.
(15) Ludi, A.; Güdel, H. U. *Structure and Bonding*; Springer-Verlag: Berlin, 1973; pp 1−21.
(16) Ohba, M.; Maruono, N.; Okawa, H.; Enoki, T.; Latour, J.-M. *J. Am. Chem. Soc.* **1994**, *116*, 11566.
(17) Miyasaka, H.; Matsumoto, N.; Okawa, H.; Re, N.; Gallo, E.; Floriani, C. *Angew. Chem., Int. Ed. Engl.* **1995**, *34*, 1446.
(18) Miyasaka, H.; Matsumoto, N.; Okawa, H.; Re, N.; Gallo, E.; Floriani, C. *J. Am. Chem. Soc.* **1996**, *118*, 981.
(19) Ohba, M.; Okawa, H.; Fukita, N.; Hashimoto, Y. *J. Am. Chem. Soc.* **1997**, *119*, 1011.
(20) Ohba, M.; Usuki, N.; Fukita, N.; Okawa, H. *Angew. Chem., Int. Ed.* **1999**, *38*, 1795.

10.1021/cm0600879 CCC: $33.50
Published on Web 04/14/2006

synthetic approach limits the number of sites available for hexacyanometalate N-coordination. This leads generally to coordination polymers with lower magnetic connectivity and dimensionality that can be interesting vacancy-free objects for low-dimensional magnetism.[24] As compared to PBs, there is a possibility of fine-tuning the magnetic properties of the bimetallic assembly via structural modification of the chelating ligand. A high number of two-dimensional (2D)[17−19,25−36] and one-dimensional[16,36−41] structures of formula $[M'(L)_n]_y[M(CN)_6]_x$ ($n = 1, 2$) have been obtained. In these compounds, the ligand can also play a functional role by introducing a molecular property in the magnetic system, such as chirality. Coexistence of chirality and magnetic order has been achieved in some cases[42−47] and may lead to interesting cross-effects, such as magnetochiral dichroism.[48] With respect to other methods based on the chiral configuration of the metal center, this ligand-induced approach has the main advantage of avoiding racemization. In a preliminary work, we have reported on the coexistence of ferromagnetic order and structural chirality in the enantiopure layered compounds $[Ni(L)_2]_3[Fe(CN)_6]_2$, where L is the chiral ligand *trans*-cyclohexane-1,2-diamine (*trans*-chxn).[49] The analysis of the magnetic properties of this system, either in its enantiopure or racemic forms, revealed an unusual magnetic behavior in the ferromagnetically ordered region.[50] The aim of the present work is to clarify the low-dimensional origin of these peculiar magnetic properties by a thorough magnetic study of the racemic system $[Ni(trans\text{-}chxn)_2]_3[Fe(CN)_6]_2$ and its comparison with the achiral 2D compound $[Ni(cis\text{-}chxn)_2]_3[Fe(CN)_6]_2$.

Experimental Section

Synthesis. *General Remarks and Chemicals.* The reagents $NiCl_2 \cdot 6H_2O$ (Fluka); $[Ni(H_2O)_6](ClO_4)_2$ (Fluka); $K_3[Fe(CN)_6]$ (Fluka); cyclohexane-1,2-diamine, 90% mixture of cis and trans (Aldrich); *trans*-(1*S*,2*S*)-chxn (Fluka); and *trans*-(1*R*,2*R*)-chxn (Fluka) were used without further purification. All the reactions were performed under ambient conditions. All products were kept away from light. The perchlorate salt must be handled with caution because it is potentially explosive.

$[Ni(cis\text{-}(1R,2S)\text{-}chxn)_2]Cl_2$ and $[Ni(trans\text{-}(1R,2R)\text{-}chxn)(trans\text{-}(1S,2S)\text{-}chxn)(H_2O)_2]Cl_2$. These precursors were obtained according to the optimized Saito and Kidani method,[51] developed by Gerard et al.[52] A solution of chxn (5 mL, 37.7 mmol) in methanol (32 mL) was added dropwise to a round-bottom flask containing $NiCl_2 \cdot 6H_2O$ (5.2 g, 21.9 mmol) in methanol (88 mL). The green solution gradually turned blue. The reaction mixture was heated at 35 °C for 20 min after which the precipitated yellow solid $[Ni(cis\text{-}(1R,2S)\text{-}chxn)_2]Cl_2$ was filtered off. It was washed with methanol (2 × 5 mL) and air-dried (yield: 1.4 g). ESI-MS: $[2L + Ni + Cl]^+$ calcd for $C_{12}H_{28}ClN_4Ni^+$, 321.13; found, 320.63; $[2L + Ni - H]^+$ calcd for $C_{12}H_{27}N_4Ni^+$, 285.16; found, 284.85. Anal. Calcd for $C_{12}H_{28}Cl_2N_4Ni$: C, 40.26; H, 7.88; N, 15.65. Found: C, 40.02; H, 8.61; N, 15.73. IR (KBr, cm^{-1}): ν = 3170, 3068 (N—H), 2929, 2858 (C—H), 1603, 1588 (N—H).

The blue filtrate was acidified with 6 M HCl (7 mL). The resulting green solution of pH 5−6 was brought to pH 6−7 with 15% NaOH (8 mL) during which the color changed to greenish blue and a violet precipitate started to appear. After prolonged cooling the solid was collected by filtration and air-dried (yield: 4 g). ESI-MS: $[2L + Ni + Cl]^+$ calcd for $C_{12}H_{28}ClN_4Ni^+$, 321.13; found, 320.82; $[2L + Ni - H]^+$ calcd for $C_{12}H_{27}N_4Ni^+$, 285.16; found, 284.79. Anal. Calcd for $C_{12}H_{32}Cl_2N_4NiO_2$: C, 36.58; H, 8.19; N, 14.22. Found: C, 36.47; H, 9.35; N, 14.30. IR (KBr, cm^{-1}): ν = 3308, 3247 (N—H), 2929, 2858 (C—H), 1603 (N—H).

$[Ni(trans\text{-}(1S,2S)\text{-}chxn)_3](ClO_4)_2 \cdot H_2O$. A solution of *trans*-(1*S*,2*S*)-chxn (1 g, 8.8 mmol) in water (10 mL) was added dropwise to a stirred solution of $[Ni(H_2O)_6](ClO_4)_2$ (1.07 g, 2.9 mmol) in the same amount of water. A violet precipitate appeared immediately. It was filtered off, washed with water, and air-dried (yield: 93%). ESI-MS: $[3L + Ni + ClO_4]^+$ calcd for $C_{18}H_{42}ClN_6NiO_4^+$, 499.23; found, 498.63; $[2L + Ni + ClO_4]^+$ calcd for $C_{12}H_{28}ClN_4NiO_4^+$, 385.11; found, 384.58; $[2L + Ni - H]^+$ calcd for $C_{12}H_{27}N_4Ni^+$, 285.16; found, 284.57; $[3L + Ni]^{2+}/z$ calcd for

(21) Ohba, M.; Okawa, H. *Coord. Chem. Rev.* **2000**, *198*, 313.
(22) Inoue, K.; Imai, H.; Ghalsasi, P. S.; Kikuchi, K.; Ohba, M.; Okawa, H.; Yakhmi, J. V. *Angew. Chem., Int. Ed.* **2001**, *40*, 4242.
(23) Kou, H.-Z.; Gao, S.; Zhang, J.; Wen, G.-H.; Su, G.; Zheing, R. K.; Zhang, X. X. *J. Am. Chem. Soc.* **2001**, *123*, 11809.
(24) Ferbinteanu, M.; Miyasaka, H.; Wernsdorfer, W.; Nakata, K.; Sugiura, K.; Yamashita, M.; Coulon, C.; Clérac, R. *J. Am. Chem. Soc.* **2005**, *127*, 3090.
(25) Ferlay, S.; Mallah, T.; Vaissermann, J.; Bartolomé, F.; Veillet, P.; Verdaguer, M. *Chem. Commun.* **1996**, 2481.
(26) Miyasaka, H.; Matsumoto, N.; Re, N.; Gallo, E.; Floriani, C. *Inorg. Chem.* **1997**, *36*, 670.
(27) Re, N.; Crescenzi, R.; Floriani, C.; Miyasaka, H.; Matsumoto, N. *Inorg. Chem.* **1998**, *37*, 2717.
(28) Miyasaka, H.; Okawa, H.; Miyazaki, A.; Enoki, T. *Inorg. Chem.* **1998**, *37*, 4878.
(29) Colacio, E.; Domínguez-Vera, J. M.; Ghazi, M.; Kivekäs, R.; Lloret, F.; Moreno, J. M.; Stoeckli-Evans, H. *Chem. Commun.* **1999**, 987.
(30) Kou, H.-Z.; Gao, S.; Bu, W.-M.; Liao, D.-Z.; Ma, B.-Q.; Jiang, Z.-H.; Yan, S.-P.; Fan, Y.-G.; Wang, G.-L. *J. Chem. Soc., Dalton Trans.* **1999**, 2477.
(31) Kou, H.-Z.; Gao, S.; Ma, B.-Q.; Liao, D.-Z. *Chem. Commun.* **2000**, 1309.
(32) Kou, H.-Z.; Bu, W.-M.; Gao, S.; Liao, D.-Z.; Jiang, Z.-H.; Yan, S.-P.; Fan, Y.-G.; Wang, G.-L. *J. Chem. Soc., Dalton Trans.* **2000**, 2996.
(33) Marvilliers, A.; Parsons, S.; Rivière, E.; Audière, J.-P.; Kurmoo, M.; Mallah, T. *Eur. J. Inorg. Chem.* **2001**, 1287.
(34) Thétiot, F.; Triki, S.; Sala Pala, J.; Gómez-García, C. J.; Golhen, S. *Chem. Commun.* **2002**, 1078.
(35) Miyasaka, H.; Ieda, H.; Matsumoto, N.; Sugiura, K.; Yamashita, M. *Inorg. Chem.* **2003**, *42*, 3509.
(36) Coronado, E.; Giménez-Saiz, C.; Nuez, A.; Sánchez, V.; Romero, F. M. *Eur. J. Inorg. Chem.* **2003**, 4289.
(37) Re, N.; Gallo, E.; Floriani, C.; Miyasaka, H.; Matsumoto, N. *Inorg. Chem.* **1996**, *35*, 6004.
(38) Fu, D. G.; Chen, J.; Tan, X. S.; Jiang, L. J.; Zhang, S. W.; Zheng, P. J.; Tang, W. X. *Inorg. Chem.* **1997**, *36*, 220.
(39) Ohba, M.; Fukita, N.; Okawa, H. *J. Chem. Soc., Dalton Trans.* **1997**, 1733.
(40) Ohba, M.; Usuki, N.; Fukita, N.; Okawa, H. *Inorg. Chem.* **1998**, *37*, 3349.
(41) Colacio, E.; Domínguez-Vera, J. M.; Ghazi, M.; Kivekâs, R.; Klinga, M.; Moreno, J. M. *Chem. Commun.* **1998**, 1071.
(42) Caneschi, A.; Gatteschi, D.; Rey, P.; Sessoli, R. *Inorg. Chem.* **1991**, *30*, 3936.
(43) Hernández-Molina, M.; Lloret, F.; Ruiz-Pérez, C.; Julve, M. *Inorg. Chem.* **1998**, *37*, 4131.
(44) Andrés, R.; Gruselle, M.; Malézieux, B.; Verdaguer, M.; Vaissermann, J. *Inorg. Chem.* **1999**, *38*, 4637.
(45) Coronado, E.; Galán-Mascarós, J. R.; Gómez-García, C. J.; Martínez-Agudo, J. M. *Inorg. Chem.* **2001**, *40*, 113.
(46) Kumagai, H.; Inoue, K. *Angew. Chem., Int. Ed.* **1999**, *38*, 1601.
(47) Minguet, M.; Luneau, D.; Lhotel, E.; Villar, V.; Paulsen, C.; Amabilino, D. B.; Veciana, J. *Angew. Chem., Int. Ed.* **2002**, *41*, 586.
(48) Rikken, G. L. J. A.; Raupach, E. *Nature* **1997**, *390*, 493−494.
(49) Coronado, E.; Gómez-García, C. J.; Nuez, A.; Romero, F. M.; Rusanov, E.; Stoeckli-Evans, H. *Inorg. Chem.* **2002**, *41*, 4615.
(50) Bellouard, F.; Clemente-León, M.; Coronado, E.; Galán-Mascarós, J. R.; Gómez-García, C. J.; Romero, F.; Dunbar, K. R. *Eur. J. Inorg. Chem.* **2002**, 1603.
(51) Saito, R.; Kidani, Y. *Chem. Lett.* **1976**, 123.
(52) Gerard, K. J.; Morgan, J.; Steel, P. J.; House, D. A. *Inorg. Chim. Acta* **1997**, *260*, 27.

$C_9H_{21}N_3Ni_{0.5}^+$, 200.14; found, 199.91. Anal. Calcd for $C_{18}H_{44}Cl_2N_6NiO_9$: C, 34.97; H, 7.17; N, 13.59. Found: C, 34.85; H, 8.04; N, 13.80%. IR (KBr, cm^{-1}): ν = 3334, 3278 (N—H), 2934, 2858 (C—H), 1644, 1587 (N—H).

[Ni(*trans*-(1*R*,2*R*)-chxn)$_3$](ClO$_4$)$_2$·H$_2$O. Prepared as described above for [Ni(*trans*-(1*S*,2*S*)-chxn)$_3$](ClO$_4$)$_2$·H$_2$O (yield: 90%). ESI-MS: $[3L + Ni + ClO_4]^+$ calcd for $C_{18}H_{42}ClN_6NiO_4^+$, 499.23; found, 499.05; $[2L + Ni + ClO_4]^+$ calcd for $C_{12}H_{28}ClN_4NiO_4^+$, 385.11; found, 384.88; $[2L + Ni - H]^+$ calcd for $C_{12}H_{27}N_4Ni^+$, 285.16; found, 284.54; $[3L + Ni]^{2+}/z$ calcd for $C_9H_{21}N_3Ni_{0.5}^+$, 200.14; found, 199.86. Anal. Calcd for $C_{18}H_{44}Cl_2N_6NiO_9$: C, 34.97; H, 7.17; N, 13.59. Found: C, 35.04; H, 8.15; N, 14.00. IR (KBr, cm^{-1}): ν = 3329, 3278 (N—H), 2929, 2858 (C—H), 1644, 1593 (N—H).

[Ni(*cis*-(1*R*,2*S*)-chxn)$_2$]$_3$[Fe(CN)$_6$]$_2$·2H$_2$O (cis). A solution of $K_3[Fe(CN)_6]$ (0.12 g, 0.36 mmol) in water (10 mL) was added dropwise to a solution of [Ni(*cis*-(1*R*,2*S*)-chxn)$_2$]Cl$_2$ (0.19 g, 0.54 mmol) in the same amount of water. The brown precipitate was filtered off, washed with water, and air-dried (yield: 83%). Slow diffusion of the precursors either in water or in water—methanol (50:50) produced the title compound as a blossom-like noncrystalline solid. Anal. Calcd for $C_{48}H_{88}Fe_2N_{24}Ni_3O_2$: C, 43.64; H, 6.71; N, 25.44. Found: C, 43.51; H, 6.72; N, 25.46. IR (KBr, cm^{-1}): ν = 3345, 3294 (N—H), 2935, 2858 (C—H), 2126, 2110 (C≡N), 1644, 1593 (N—H).

[Ni(*trans*-(1*R*,2*R*)-chxn)(*trans*-(1*S*,2*S*)-chxn)]$_3$[Fe(CN)$_6$]$_2$·2H$_2$O (trans). Slow diffusion of [Ni(*trans*-(1*R*,2*R*)-chxn)(*trans*-(1*S*,2*S*)-chxn)(H$_2$O)$_2$]Cl$_2$ (0.11 g, 0.28 mmol) and $K_3[Fe(CN)_6]$ (0.09 g, 0.28 mmol) in water yielded brown plate-shaped single crystals. Anal. Calcd for $C_{48}H_{88}Fe_2N_{24}Ni_3O_2$: C, 43.64; H, 6.71; N, 25.44. Found: C, 43.39; H, 6.65; N, 25.28. IR (KBr, cm^{-1}): ν = 3339, 3288 (N—H), 2930, 2863 (C—H), 2115 (C≡N), 1639, 1598 (N—H).

[Ni(*trans*-(1*S*,2*S*)-chxn)$_2$]$_3$[Fe(CN)$_6$]$_2$·2H$_2$O (SS). To a solution of [Ni(*trans*-(1*S*,2*S*)-chxn)$_3$](ClO$_4$)$_2$·H$_2$O (0.1 g, 0.17 mmol) in a 50:50 water—acetonitrile mixture (40 mL) was added [Ni(H$_2$O)$_6$](ClO$_4$)$_2$ (0.006 g, 0.017 mmol), followed by the dropwise addition of an aqueous (20 mL) solution of $K_3[Fe(CN)_6]$ (0.056 g, 0.17 mmol). Dark brown crystals formed over the next few days. Single crystals were grown by slow diffusion of the precursors in water—acetonitrile. Anal. Calcd for $C_{48}H_{88}Fe_2N_{24}Ni_3O_2$: C, 43.64; H, 6.71; N, 25.44. Found: C, 43.56; H, 6.49; N, 25.26. IR (KBr, cm^{-1}): ν = 3339, 3278 (N—H), 2919, 2848 (C—H), 2120, 2105(C≡N), 1634, 1588 (N—H).

[Ni(*trans*-(1*R*,2*R*)-chxn)$_2$]$_3$[Fe(CN)$_6$]$_2$·2H$_2$O (RR). RR was prepared starting from [Ni(*trans*-(1*R*,2*R*)-chxn)$_3$](ClO$_4$)$_2$·H$_2$O as described above for **SS**. Anal. Calcd for $C_{48}H_{88}Fe_2N_{24}Ni_3O_2$: C, 43.64; H, 6.71; N, 25.44. Found: C, 43.46; H, 6.63; N, 25.34. IR (KBr, cm^{-1}): ν = 3334, 3283 (N—H), 2925, 2858 (C—H), 2120, 2105 (C≡N), 1634, 1588 (N—H).

Mössbauer Spectroscopy. ^{57}Fe Mössbauer measurements were recorded in transmission mode using a conventional constant acceleration spectrometer and a 25 mCi ^{57}Co source in a Rh matrix. Powdered samples were packed in Perspex holders to obtain Mössbauer absorbers containing approximately 5 mg/cm^2 of natural iron. The velocity scale was calibrated using an α-Fe foil at room temperature. Isomer shift (IS) values are given relative to this standard. Spectra were collected with the absorbers between 295 and 5 K. Low-temperature measurements were obtained using a flow cryostat with a temperature stability of ±0.5 K. The spectra were fitted to Lorentzian lines using a nonlinear least-squares fitting method.[53]

Magnetic Measurements. Magnetic properties of **trans** (multiple plate-shaped crystals, 19.84 mg) and **cis** (powder sample, 18.02 mg) were collected with a superconducting quantum interference device magnetometer (Quantum Design MPMS-XL-5). Temperature dependences of magnetization were measured in the 2—300 K range under a 1000 Oe direct current (dc) field. Diamagnetic contributions of the compounds were calculated from Pascal constants. The procedure for measuring zero-field-cooled (ZFC), field-cooled (FC), and remanent magnetizations of **trans** was as follows. The remanent magnetic field was canceled out at room temperature, and the sample was cooled to 2 K in zero field. At 2 K an external magnetic field (H_{dc} = 1, 50, 250, and 1000 Oe) was applied, and M_{ZFC} was measured while heating to 30 K. The sample was kept at this temperature for 20 min, after which M_{FC} was measured from 30 to 2 K. Once at 2 K, H_{dc} was set to 0 and M_{rem} was registered while increasing the temperature to 30 K. Isothermal magnetizations and alternating current (ac) susceptibilities of **trans** were measured after cooling the sample in zero field. Specific heat experiments of **trans** (six randomly oriented single crystals, 0.22 mg) and **cis** (powder sample, 1.90 mg) at constant pressure were performed using a physical properties measurement system (Quantum Design PPMS-9).

Results and Discussion

Synthesis. Ligand chxn (Scheme 1) possess two stereogenic centers and exists in two diastereomeric forms: the cis isomer is an achiral meso form, while the trans isomer may exist as a racemic mixture (*trans-rac*-chxn) or may be resolved in its enantiomers *trans*-(1*S*,2*S*)-chxn and *trans*-(1*R*,2*R*)-chxn. Both enantiomers are commercially available and form optically active [Ni(*trans*-(1*S*,2*S*)-chxn)$_3$](ClO$_4$)$_2$·H$_2$O and [Ni(*trans*-(1*R*,2*R*)-chxn)$_3$](ClO$_4$)$_2$·H$_2$O complexes in near quantitative yields. These salts can be used in the preparation of chiral cyano-bridged bimetallic assemblies. Slow interdiffusion of aqueous acetonitrile solutions of the corresponding tris-chelated Ni(II) complex and $K_3[Fe(CN)_6]$ yields the optically active heterometallic compounds [Ni(*trans*-(1*S*,2*S*)-chxn)$_2$]$_3$[Fe(CN)$_6$]$_2$·2H$_2$O (**SS**) and [Ni(*trans*-(1*R*,2*R*)-chxn)$_2$]$_3$[Fe(CN)$_6$]$_2$·2H$_2$O (**RR**) as single crystals suitable for X-ray diffraction.

When a mixture of *cis*- and *trans-rac*-chxn reacts with NiCl$_2$·6H$_2$O, two different solids can be easily separated:[51] the square planar [Ni(*cis*-chxn)$_2$]Cl$_2$ complex and the *trans*-diaqua octahedral racemic complex [Ni(*trans-rac*-chxn)$_2$(H$_2$O)$_2$]Cl$_2$. These two nickel(II) compounds can also be used as building blocks for the construction of bimetallic materials. Thus, slow diffusion of water solutions of these metal precursors into a water solution of $K_3[Fe(CN)_6]$ affords, respectively, achiral [Ni(*cis*-chxn)$_2$]$_3$[Fe(CN)$_6$]$_2$·2H$_2$O (**cis**) and racemic [Ni(*trans-rac*-chxn)$_2$]$_3$[Fe(CN)$_6$]$_2$·2H$_2$O (**trans**).

Chiroptical Properties. The enantiopure tris-chelated precursors [Ni(*trans*-(1*S*,2*S*)-chxn)$_3$](ClO$_4$)$_2$·H$_2$O and [Ni(*trans*-(1*R*,2*R*)-chxn)$_3$](ClO$_4$)$_2$·H$_2$O exhibit identical optical absorption spectra in the 300—800 nm range. As expected for octahedrally coordinated Ni(II) complexes, three d—d bands are observed at 339 nm ($^3A_{2g} \rightarrow {}^3T_{1g}(P)$), 542 nm ($^3A_{2g} \rightarrow {}^3T_{1g}(F)$), and 856 nm ($^3A_{2g} \rightarrow {}^3T_{2g}(F)$). Crystal field parameters obtained from these data are typical of tris-diamine Ni(II) complexes: Δ = 11 680 cm^{-1} and B = 860 cm^{-1}. Circular dichroism (CD) spectra show that the three

(53) Waerenborgh, J. C.; Figueiredo, M. O.; Cabral, J. M. P.; Pereira, L. C. J. *J. Solid State Chem.* **1994**, *111*, 300.

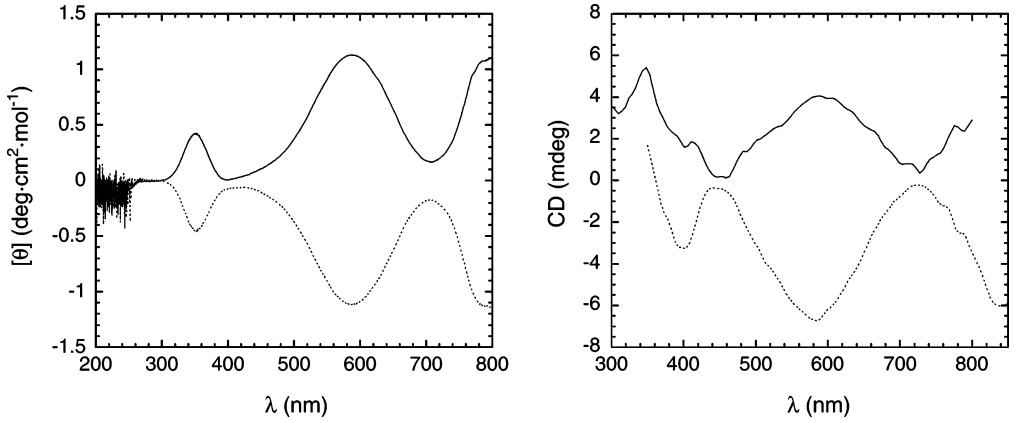

Figure 1. (a) CD spectra of acetonitrile−water solutions of the bis-chelated precursors [Ni(*trans*-(1*R*,2*R*)-chxn)$_2$(H$_2$O)$_2$](ClO$_4$)$_2$ (solid line) and [Ni(*trans*-(1*S*,2*S*)-chxn)$_2$(H$_2$O)$_2$](ClO$_4$)$_2$ (dotted line). (b) CD spectra of powdered samples of **RR** (solid line) and **SS** (dotted line) in a KBr matrix.

Scheme 1

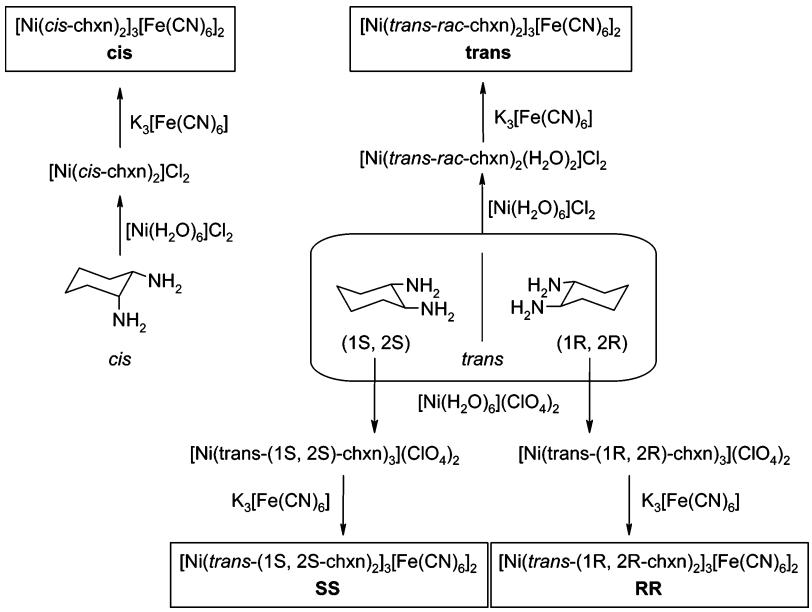

absorption bands are dichroic, showing opposite Cotton effects for [Ni(*trans*-(1*S*,2*S*)-chxn)$_3$](ClO$_4$)$_2$·H$_2$O and [Ni(*trans*-(1*R*,2*R*)-chxn)$_3$](ClO$_4$)$_2$·H$_2$O complexes. The low-energy band is magnetically allowed in octahedral symmetry, and it is thus intensely dichroic, with a positive Cotton effect for the (1*R*,2*R*) compound. The intermediate band is split into two components, probably because of spin−orbit coupling, and it exhibits a negative Cotton effect for the (1*R*,2*R*) compound. Finally, the nominally forbidden high-energy band is also split into two components of opposite sign.[54]

The corresponding bis-chelated precursors [Ni(*trans*-(1*S*,2*S*)-chxn)$_2$(H$_2$O)$_2$](ClO$_4$)$_2$ and [Ni(*trans*-(1*R*,2*R*)-chxn)$_2$(H$_2$O)$_2$](ClO$_4$)$_2$ also show three absorption bands in the visible region, centered at 348 nm ($^3A_{2g} \rightarrow {}^3T_{1g}(P)$), 555 nm ($^3A_{2g} \rightarrow {}^3T_{1g}(F)$), and 880 nm ($^3A_{2g} \rightarrow {}^3T_{2g}(F)$). Crystal field parameters derived from these data ($\Delta = 11\,360$ cm^{-1} and $B = 840$ cm^{-1}) are in agreement with the replacement of one stronger chxn ligand by two water molecules in the nickel(II) coordination sphere. In the CD spectra the electronic transitions appear at higher wavelengths (353 and 588 nm for the two high-energy bands). The three absorption bands show a positive Cotton effect for the (1*R*,2*R*) complex (Figure 1a). As compared to the tris-chelated precursors, the low-energy dichroic signals are considerably weaker, possibly because of a more pronounced deviation from octahedral symmetry. In contrast, the initially forbidden higher-energy bands become relatively stronger. The bis-chelated complexes are good models for comparison with the CD properties of the bimetallic compounds **SS** and **RR**. Indeed, CD spectra of these two chiral NiFe compounds in the solid state exhibit also three dichroic signals in the visible region (Figure 1b). The intermediate band lies exactly at the same wavelength (585 nm), and it corresponds to the $^3A_{2g} \rightarrow {}^3T_{1g}(F)$ electronic transition. The low-energy band is located outside the range of the spectrum, as it was also the case for the nickel(II) precursors. Further, a positive Cotton effect is also observed for the three bands of **RR**. The only divergence is detected around 400 nm, where a dichroic signal related to a strong CT absorption band is found.

Crystal Structures of RR, SS, and trans. Compounds **RR** and **SS** are enantiomorphs (they are mirror images of each other but are not identical) and crystallize in the

(54) Treptow, R. S. *Inorg. Chem.* **1968**, *7*, 1229.

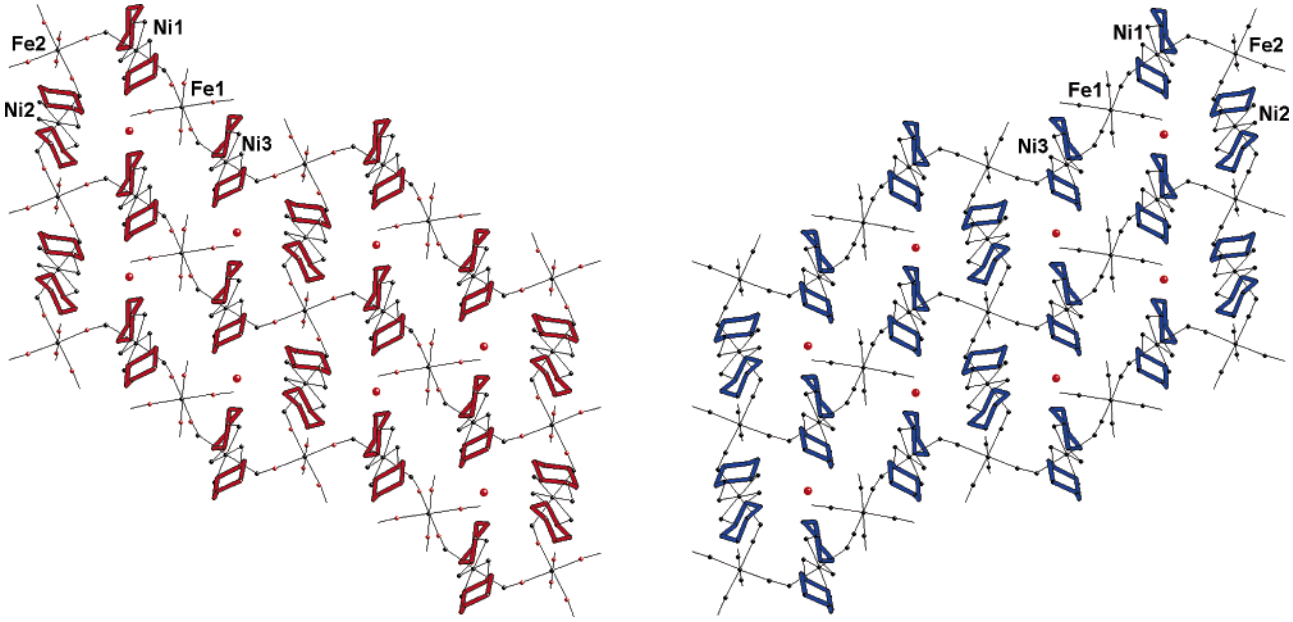

Figure 2. View of the crystal structures of **SS** (left) and **RR** (right) along the *y* direction showing the numbering scheme for significant atoms. Note that one structure is the mirror image of the other. Selected bond distances and angles: Ni1−NC(Fe1), 2.090(9) Å; Ni1−NC(Fe2), 2.166(9) Å; Ni2−NC(Fe2), 2.145(9) Å; Ni2−NC(Fe2), 2.138(9) Å; Ni3−NC(Fe1), 2.105(8) Å; Ni3−NC(Fe2), 2.194(9) Å; Ni1−N−C(Fe1), 150.3(8)°; Ni1−N−C(Fe2), 128.6(9)°; Ni2−N−C(Fe2), 121.2(8)°; Ni2−N−C(Fe2), 125.0(8)°; Ni3−N−C(Fe1), 146.6(8)°; Ni3−N−C(Fe2), 128.0(9)°.

noncentrosymmetric *P*1 space group[49] (Figure 2). Their structures can be described as layers of dodecanuclear cyclic units in which alternating *trans*-[Ni(*trans*-chxn)$_2$] cations and $[Fe(CN)_6]^{3-}$ anions are linked by CN^- bridges ((12, 4) topology). Two types of iron atoms (Fe1 and Fe2) are found: Fe2 binds to four adjacent Ni(II) centers in the same plane via cyanide bridges, whereas Fe1 corresponds to a $[Fe(CN)_6]^{3-}$ anion that is connected linearly to two *trans*-[Ni(*trans*-chxn)$_2$] moieties and hydrogen-bonded to two water molecules. It is worth mentioning the extremely bent Ni−N−C angles (with values ranging between 150.3 and 121.2°) as compared to those of similar compounds.[16,19,29−32,39,40,55−59] Chirality is introduced in the structures owing to the presence of the *trans*-chxn ligands (only one enantiomeric form is present in the structure of each compound). **RR** contains [Ni(*trans*-(1*R*,2*R*)-chxn)$_2$] units in which all chelate rings adopt the same λ conformation. A δ conformation is correspondingly found in the [Ni(*trans*-(1*S*,2*S*)-chxn)$_2$] fragments of **SS**. A view parallel to the layers (Figure 3) shows that all iron atoms and Ni2 lie in the same *ac* plane, while Ni1 and Ni3 are located at 0.800(3) Å above and 0.921(2) Å below this plane, respectively. The bulky cyclohexane rings are also arranged at both sides of the layer, giving rise to a large interplane distance of 11.752 Å. The crystal structure of **trans** is very similar. Now the two enantiomers *trans*-(1*R*,2*R*)-chxn and *trans*-(1*S*,2*RS*)-chxn are randomly distributed over the crystal lattice. This results in a centrosymmetric structure ($P\bar{1}$ space group).[50]

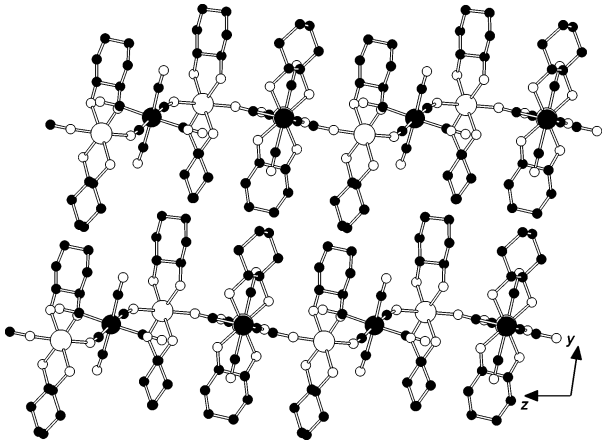

Figure 3. Projection of the crystal structure of **RR** onto the bc plane showing the arrangement of the layers in the *y* direction.

Mössbauer Spectroscopy. Mössbauer spectra taken between 16 and 295 K show one quadrupole doublet for **cis** and two for **trans** (Figure 4). The estimated IS values (Table 1) are typical of low-spin ferricyanide anions.[60,61] The two different quadrupole splittings observed for **trans** are consistent with the two different coordinations of Fe deduced from the crystal structure determination. The fact that only one quadrupole doublet is observed for **cis**, whose structure is still unknown, suggests that only one type of Fe coordination site exists in this compound.

Spectra recorded below 10 K (Figure 4) show magnetic multiplets, indicating a drastic slowing down of the relaxation of the Fe magnetic moments. In agreement with magnetization data (see below) this decrease of the relaxation may be explained by the establishment of cooperative magnetic ordering.

(55) Ohba, M.; Okawa, H.; Ito, T.; Ohto, A. *J. Chem. Soc., Chem. Commun.* **1995**, 1545.
(56) Salah El Fallah, M.; Rentschler, E.; Caneschi, A.; Sessoli, R.; Gatteschi, D. *Angew. Chem., Int. Ed. Engl.* **1996**, *35*, 1947.
(57) Zhang, S.-W.; Fu, D.-G.; Sun, W.-Y.; Hu, Z.; Yu, K.-B.; Tang, W.-X. *Inorg. Chem.* **2000**, *39*, 1142.
(58) Colacio, E.; Domínguez-Vera, J. M.; Lloret, F.; Rodríguez, A.; Stoeckli-Evans, H. *Inorg. Chem.* **2003**, *42*, 6962.
(59) Saha, M. K.; Morón, M. C.; Palacio, F.; Bernal, I. *Inorg. Chem.* **2005**, *44*, 1354.
(60) Iijima, S.; Honda, Z.; Koner, S.; Mizutani, F. *J. Magn. Magn. Mater.* **2001**, *223*, 16.
(61) Bonadio, F.; Senna, M.-C.; Ensling, J.; Sieber, A.; Neels, A.; Stoeckli-Evans, H.; Decurtins, S. *Inorg. Chem.* **2005**, *44*, 969.

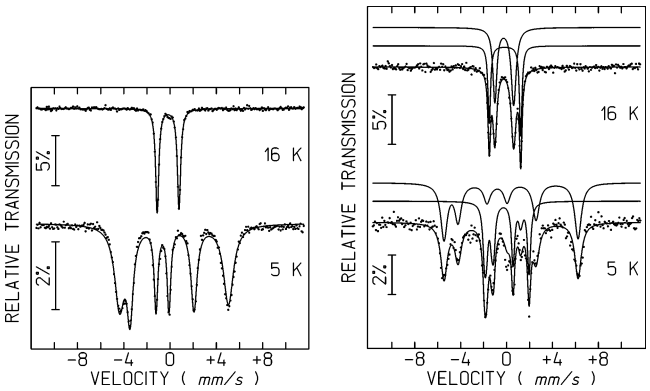

Figure 4. Mössbauer spectra of **cis** (left) and **trans** (right). The lines over the experimental points are the calculated functions corresponding to the sum of the contributions of the different Fe centers. Individual contributions are shown slightly shifted for clarity.

Table 1. Estimated Parameters from the Mössbauer Spectra of cis and trans at Different Temperatures above T_C

T	IS	Δ	Γ	I
		cis		
295 K	−0.15	1.54	0.33	100
50 K	−0.06	1.88	0.33	100
13 K	−0.05	1.91	0.40	100
		trans		
295 K	−0.12	2.48	0.27	41
	−0.18	1.30	0.25	59
165 K	−0.06	2.65	0.26	40
	−0.13	1.46	0.30	60
101 K	−0.05	2.69	0.24	41
	−0.11	1.52	0.30	59
16 K	−0.03	2.74	0.25	39
	−0.09	1.64	0.40	61

[a] IS (mm/s), IS relative to metallic α-Fe at 295 K; Δ (mm/s), quadrupole splitting; Γ (mm/s), line width; I, relative area. Estimated errors are ≤ 0.02 mm/s for IS, Δ, and Γ and <2% for I.

The simplest spectrum is the six-peak pattern observed for **cis**. This simple pattern is again consistent with a single Fe site. However, the spacing between the lines does not allow a fit by a simple magnetic sextet. As a result of the low symmetry of the site where Fe is located, probably similar to the symmetry of the Fe sites in **trans**, the quadrupole hyperfine interaction cannot be treated as a perturbation of the magnetic hyperfine interaction and the magnetic sextet approximation is not valid. The position and relative intensities of the absorption lines of the magnetically ordered Fe atoms were therefore calculated by solving the complete Hamiltonians for the hyperfine interactions in both the excited and the ground nuclear states of the ^{57}Fe nuclei.[62] A very good agreement of the calculated and observed line positions is obtained with the parameters summarized in Table 2. To obtain a good fit of the intensities, peaks with the higher calculated areas should have significantly higher line widths, while those with the lower calculated areas should be significantly narrower. This may be related to saturation effects. However, considering that both peaks with the highest calculated areas are those corresponding to the lowest and highest nuclear transition energies, a narrow distribution of hyperfine fields due to some heterogeneity in the distribution of water molecules inside the structure cannot be discarded.

(62) Ruebenbauer, K.; Birchall, T. *Hyperfine Interact.* **1979**, *7*, 125.

Table 2. Estimated Parameters from the Mössbauer Spectra of cis and trans at 5 K[a]

IS	Δ¢	η	B_{hf}	θ	φ	I
			cis			
−0.05	−2.14	−0.3	28(1)	84°	31°	100
			trans			
−0.02	−2.59	0.5	5.1(1)	90°	55°	40
−0.11	−1.35	−0.8	36(1)	90°	179°	60

[a] IS and I as in Table 1. $\Delta' = e^2QV_{zz}/2$ (mm/s), quadrupole interaction; B_{hf} (T), magnetic hyperfine field. Estimated errors are ≤ 0.02 mm/s for IS and Δ; <0.2 T for B_{hf}; and <3% for I. θ and φ, the polar and azimuthal angles of B_{hf} relative to the main axes of the EFG, as well as η, the asymmetry parameter, were kept constant during the fitting procedure. Values in the table correspond to the best-fit data.

The spectrum obtained at 5 K for **trans** is more complex than the former one, which is not surprising considering that at least two multiplets, corresponding to the two doublets observed at higher temperatures, should be observed. The peaks in the lowest and highest velocity ranges of the spectra suggest that a multiplet similar to that observed for **cis** should be present. The calculated parameters corresponding to the best fit are shown in Table 2. Considering that the lines that still have to be fitted are in a much smaller velocity range around the center of the spectrum, the second multiplet should have a much lower magnetic hyperfine field, B_{hf}, as confirmed by the calculated parameters.

In **trans** the doublet and the multiplet with similar relative areas, I, also have approximately the same IS, thus showing that the analyses of the spectra above and below T_C are consistent. The doublet with $I \sim 40\%$ also has the largest quadrupole interactions (Tables 1 and 2). Large quadrupole splittings, exceeding 2 mm/s, are usually associated with $[Fe(CN)_6]^{3-}$ units coordinated by two bridging CN^- groups in trans positions and four terminal CN^- groups.[60] The component with $I \sim 60\%$ should therefore be attributed to the Fe site with four bridging CN^- anions (Fe2). Below T_C the multiplet with $I \sim 40\%$ has a significantly lower B_{hf} than the other one (Table 2). This may be related to the fact that Fe1 atoms have a lower number of Ni neighbors, as compared to Fe2, thus decreasing the magnetic exchange interactions. Note that the intensity ratio between the two multiplets (60:40) differs from the expected value (50:50). This might be due to texture effects or to a faster relaxation of the low-intensity component.

Structure of cis. The Fe atoms in **cis** have IS values intermediate between those of the two nonequivalent Fe atoms found in **trans**. Considering that all Fe sites are equivalent and given the Ni_3Fe_2 stoichiometry, an iron coordination sphere consisting of three bridging and three terminal cyanide anions can be safely postulated. On the other hand, the bulky chxn ligand has a strong tendency to give bis-chelated complexes with a trans configuration. Under *both* circumstances, there are only two possible crystal structures depending on the relative arrangement of the bridging cyanides: a facial arrangement leads to a corrugated 2D honeycomb-like structure whereas a meridional arrangement yields a flat 2D brick-wall-like system (Figure 5).[29−32] The powder X-ray diffractogram of **cis** shows an intense peak at low angles that might be attributed to the interlayer spacing of the 2D system. Indeed, this peak (θ =

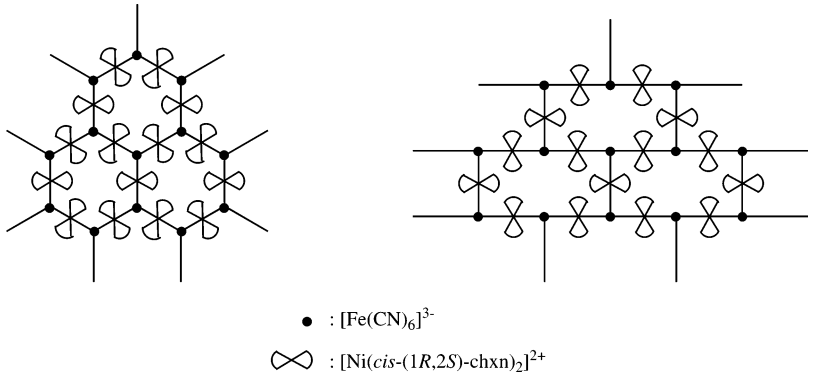

Figure 5. Representation of the two possible layered structures (honeycomb- and brick-wall-like) of **cis**.

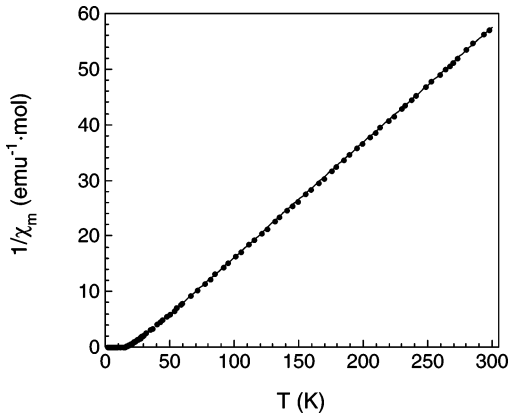

Figure 6. Thermal dependence of the reciprocal molar susceptibility of **trans**. The solid line corresponds to the fit to the Curie−Weiss law in the 50−300 K region.

7.82°; $d = 11.299$ Å) compares well with the low-angle peak obtained from the simulated powder X-ray diffractogram of 2D **trans** ($\theta = 7.57°$; $d = 11.672$ Å). This also demonstrates that in both structures the chxn ligands are located at both sides of the bimetallic layers, determining the interlayer spacing. Thus, the structure of **cis** is likely to be 2D, either planar or corrugated.

Magnetic Properties of trans. *Results.* Magnetic susceptibility measurements for the different stereoisomers derived from *trans*-chxn were undertaken. All of them exhibit similar magnetic properties. In the following, we will only refer to the racemate **trans**. Figure 6 gives the thermal dependence of its inverse susceptibility. For temperatures above 50 K, the susceptibility follows a Curie−Weiss law with parameters $C = 4.8$ emu·K·mol^{-1} and $\theta = 21.7$ K. The Curie constant, C, is very close to the calculated value for uncorrelated Ni^{2+} ($S = 1$; $g = 2.15$) and low-spin Fe^{3+} ($S = 1/2$; $g = 2.7$) centers ($C = 4.8$ emu·K·mol^{-1}, g values are similar to those reported for previous NiFe cyanide-bridged systems). The θ parameter indicates relatively strong ferromagnetic interactions between these spin carriers. The thermal variation of the χT product (Supporting Information) is nearly constant at room temperature (5.2 emu·K·mol^{-1}). Upon cooling, χT increases monotonically in the paramagnetic region and diverges to a maximum value of 361 emu·K·mol^{-1} in the ordered region.

Magnetization measurements in the 2−30 K range have been obtained in the ZFC and FC modes, at different values of the applied field. Below 16 K, M shows an abrupt increase with decreasing temperature (Figure 7), reaching saturation at lower T values. Irrespective of the field conditions, a critical temperature $T_c = 14.3 \pm 0.3$ K can be obtained from the first derivative of the M versus T curve. In the ordered phase, a strong magnetic hysteresis between the ZFC and FC modes is observed. In very small fields (1 Oe), the ZFC curve exhibits a rounded maximum at $T_p = 12.4$ K and falls down below $T = 6$ K. In higher fields, the maximum broadens and vanishes as the field exceeds 250 Oe. The other feature shifts to lower temperatures and also disappears at higher field values (1000 Oe). The point of irreversibility, T_{irr}, where ZFC and FC curves split, shifts also to lower temperatures as the field increases. The thermomagnetic irreversibility is usually considered as a fingerprint of superparamagnetic or glassy behavior.[63−66] Note, however, that any magnetically ordered phase with a net magnetic moment might be irreversible due to the formation of magnetic domains.[67−69] The domain walls move easily under an applied field during the FC process, thus increasing the size of the domains with magnetization parallel to the field and the total magnetization of the sample. After a ZFC process, the random orientation of the magnetic domains is frozen. When the magnetic field is applied to such a system at low temperatures, its energy may not be enough to unblock the domain-wall movement, so that $M_{ZFC} < M_{FC}$. Increasing the applied field favors the movement of the domain walls, decreasing the difference between M_{ZFC} and M_{FC}, and shifting T_{irr} to lower values.

The formation of a spontaneous moment was probed by warming the sample in zero field after cooling in various dc fields. The observed remanent magnetization M_{rem} (Figure 8) drops steadily in the 2−5 K range, diminishes gradually until T approaches T_{irr}, and then vanishes abruptly. From the inflection point of the $M_{rem} = f(T)$ curve at 1 Oe, a T_c of 14.0 K is obtained, in agreement with the FC magnetization study. To determine the nature of the magnetic transition,

(63) DeFotis, G. C.; Coffey, G. A.; Cinquina, C. C.; Chandarlapaty, S.; Brubaker, W. W.; Krovich, D. J.; Chamberlain, R. V.; Jarvis, W. R. A. *Phys. Rev. B* **1995**, *51*, 15113.
(64) Zhang, J. H.; Chen, F.; Li, J.; O'Connor, C. J. *J. Appl. Phys.* **1997**, *81*, 5283.
(65) Gîrţu, M. A.; Wynn, C. M.; Fujita, W.; Awaga, K.; Epstein, A. J. *J. Appl. Phys.* **1998**, *83*, 7378.
(66) Lafond, A.; Meerschaut, A.; Rouxel, J.; Tholence, J. L.; Sulpice, A. *Phys. Rev. B* **1995**, *52*, 1112.
(67) Anil Kumar, P. S.; Joy, P. A.; Date, S. K. *Physica B* **1999**, *269*, 356.
(68) Chernova, N. A.; Song, Y.; Zavalij, P. Y.; Whittingham, M. S. *Phys. Rev. B* **2004**, *70*, 144405.
(69) Balanda, M.; Szytuła, A.; Guillot, M. *J. Magn. Magn. Mater.* **2002**, *247*, 345.

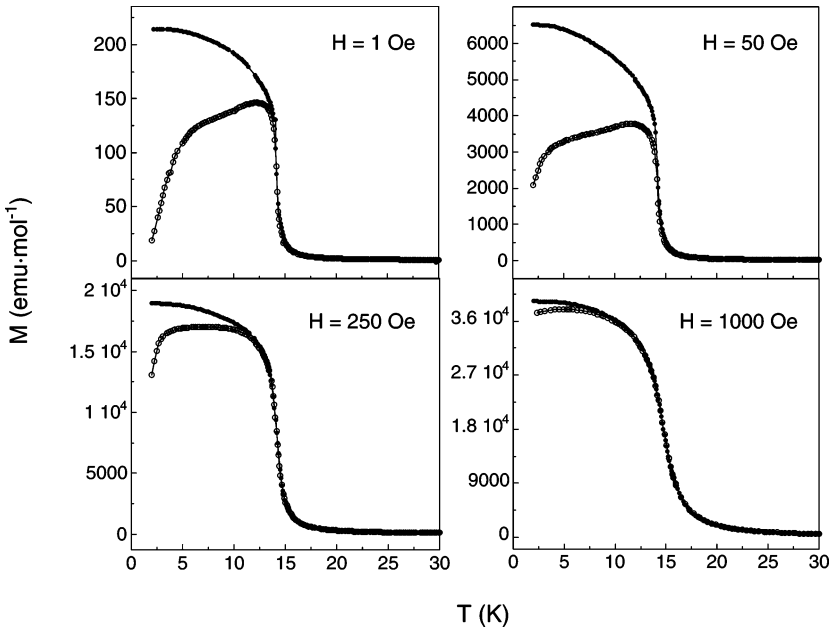

Figure 7. ZFC (open circles) and FC (solid circles) curves of **trans** at applied fields of 1, 50, 250, and 1000 Oe.

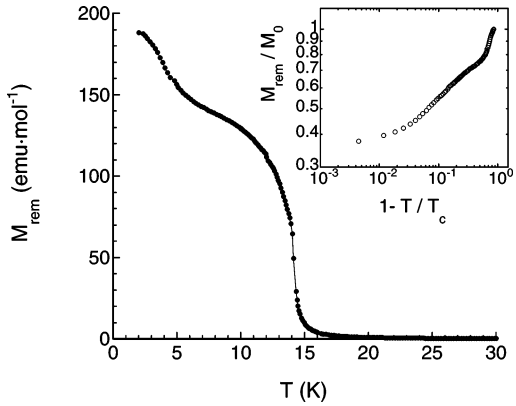

Figure 8. Thermal variation of the remanent magnetization of **trans** after a FC measurement at 1 Oe. Inset: Double logarithmic plot of M_{rem}/M_0 versus the reduced temperature for temperatures below T_c.

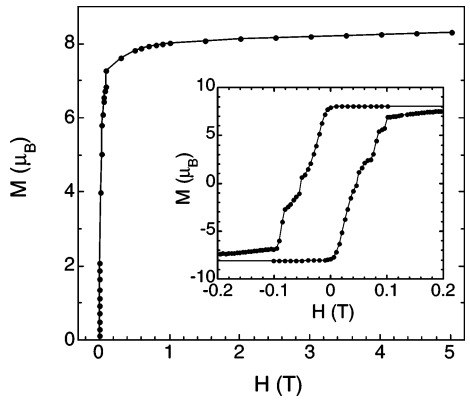

Figure 9. First magnetization curve of **trans** at 2 K after cooling in zero field. Inset: Hysteresis plot measured at the same temperature.

we have performed a critical analysis (see inset Figure 8). The fit of the low-field remanent magnetization to the power law $M_{rem} = M_0(1 - T/T_c)^{\beta}$ in the critical region ($10^{-2} < 1 - T/T_c < 10^{-1}$) gives a critical exponent $\beta_1 = 0.10$ which changes to $\beta_2 = 0.21$ at 13.5 K, upon cooling. β_1 is close to the expected value for 2D Ising magnetic systems ($\beta = 1/8$). The critical exponent at lower temperatures β_2 is still lower than that expected for a 3D Ising ferromagnet ($\beta = 0.32$). Therefore, the change in critical behavior that occurs at 13.5 K does not seem to be related to dimensionality crossover.

The field dependence of the magnetization (Figure 9) was studied at different temperatures in the 0−5 T range to investigate for possible hysteretic effects. At 2 K, the first magnetization curve shows a sharp increase at low field values. Above $H = 5000$ Oe, the magnetization grows almost linearly and does not reach saturation at the highest field of the experiment. The expected magnetization at saturation is the sum of the contribution of the Ni^{2+} ($S = 1$; $g = 2.15$) and low-spin Fe^{3+} ($S = 1/2$; $g = 2.7$) ions ($M_{sat} = 9.15\ \mu_B \cdot mol^{-1}$). Instead, a maximum value of $8.30\ \mu_B$ per formula is obtained at the highest field of the experiment (5 T), in good comparison with similar compounds. This difference is due to the magnetocrystalline anisotropy of the compound. In fact, preliminary magnetic studies on a single crystal show a very strong axial anisotropy with the easy magnetic axis lying perpendicular to the bimetallic layers. After demagnetization, a pronounced hysteresis is observed with a remanent magnetization $M_{rem} = 7.92$ emu·mol^{-1} (87% of the saturation magnetization) and a coercive field $H_c = 524$ Oe. Increasing the temperature of the experiment produces smaller coercive fields. Figure 10 shows the temperature dependence of H_c. A detectable coercive field appears below 11 K and increases linearly at a rate of 43.5 Oe/K with decreasing temperature. Below 4 K, a strong augmentation in coercivity is observed. This indicates a higher blocking of the domain walls in this temperature range.[70]

In summary, the set of dc measurements indicates a magnetic phase transition from a paramagnetic state to a ferromagnetic state at the Curie temperature $T_C = 14.0$ K. In the ordered phase, irreversibility seems to be determined by magnetic anisotropy rather than a glassy behavior, although dc data do not provide enough evidence to distinguish between these two effects. Spin glasses and

(70) Andreev, A. V. *J. Alloys Compd.* **2002**, *336*, 77.

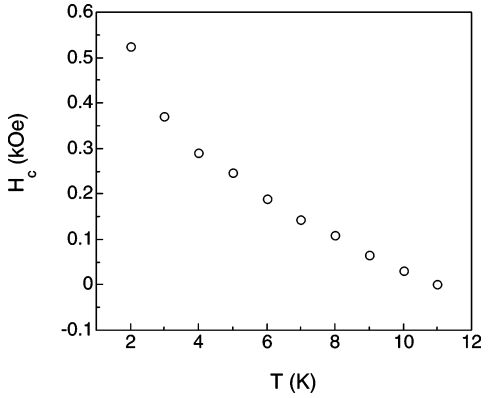

Figure 10. Temperature variation of the coercivity of **trans**.

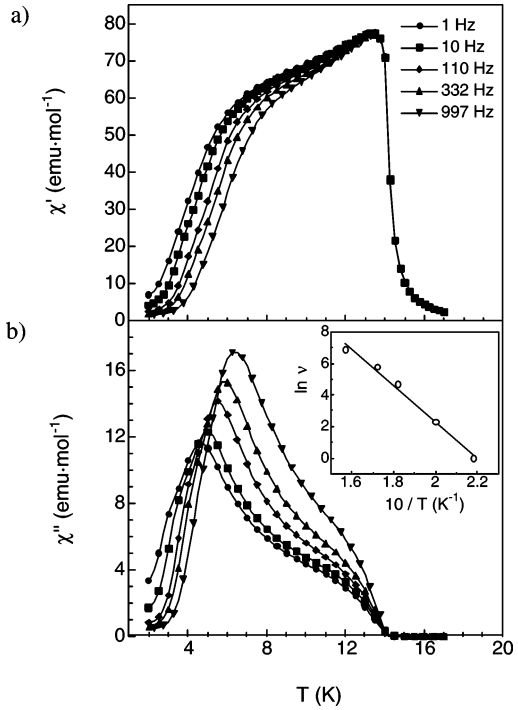

Figure 11. Thermal variation of the ac molar susceptibility of **trans** [(a) real part, χ'; (b) imaginary part, χ''] measured at frequencies of 1, 10, 110, 332, and 997 Hz (circles, squares, rhombuses, upward pointing triangles, and downward pointing triangles, respectively) in a 3.9 Oe ac magnetic field. Inset in part b: Logarithm of the frequency vs the inverse of T_{max}. The straight line represents the fit to Arrhenius law.

ferromagnets display, however, a different frequency dependence of the ac susceptibility for freezing of the spins and domains, respectively.[71,72] The temperature dependence of the real χ' and imaginary χ'' parts of the ac susceptibility of **trans** was measured in an ac driving field of 3.9 Oe at different frequencies (Figure 11). Just below T_C, the real part χ' exhibits the Hopkinson maximum and then decreases in two steps on further cooling. In an ac field oscillating at a frequency of 1 Hz, the first step lies in the 13−8 K temperature range, where χ' diminishes smoothly and reaches an inflection point at $T_i = 9.5$ K. Below 6 K, the in-phase component cancels out very rapidly, in parallel with the abrupt decrease observed in the ZFC magnetization measurement. The imaginary part χ'' appears at the Curie temperature $T_C = 14.0$ K, characterizing the phase transition from a paramagnetic to a long-range (ferromagnetic) ordered state. The out-of-phase component, which characterizes magnetic losses, grows gradually between 13 and 8 K. Below 8 K, χ'' increases steadily to reach a maximum at $T_{max} = 4.6$ K, then vanishes very abruptly. Both χ' and χ'' shift toward higher temperatures as the frequency becomes higher. The maximum of the $\chi'' = f(T)$ curve, T_{max}, is a good singular point to study this frequency dependence. The maximal relative shift per decade of frequency $\Delta T_{max}/[T_{max}\Delta(\log \nu)]$ equals 0.09, a value that is considerably higher than expected for a canonical spin glass ($10^{-2}-10^{-3}$).[73] The frequency shift of T_{max} has been fitted (Figure 11b, inset) to a thermally activated process, described by the Arrhenius law $\nu = \nu_0 \exp(-E_a/kT)$, yielding satisfactory values for the activation energy $E_a = 116$ K and $\nu_0 = 1.3 \times 10^{11}$ Hz. To fully discard the existence of glassy behavior, a fit to the Vogel−Fulcher law $\nu = \nu_0 \exp[-E_a/k(T - T_0)]$ was also attempted. For values of T_0 slightly below T_{max} (1 Hz) data did not show, in fact, a linear behavior.

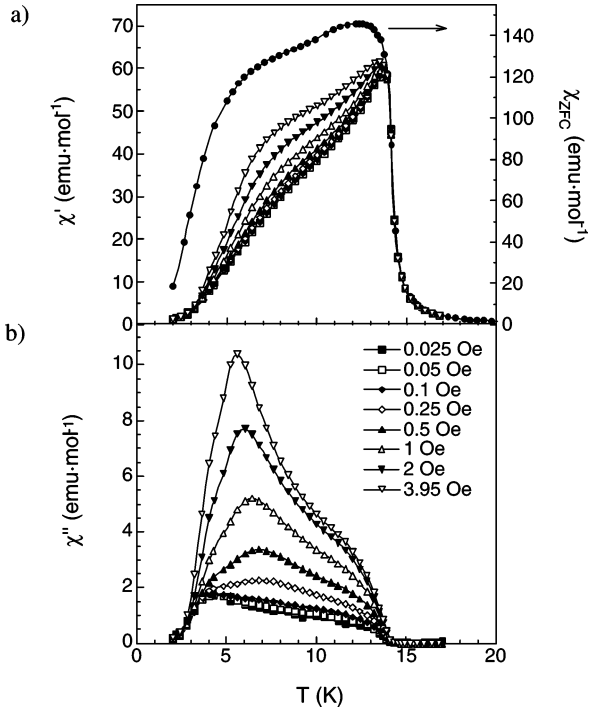

Figure 12. (a) Temperature variation of the ZFC susceptibility under a dc field of 1 Oe (full circles) and the real part of ac molar susceptibility χ' at 110 Hz under ac fields of 0.025, 0.05, 0.1, 0.25, 0.5, 1, 2, and 3.95 Oe (full and empty squares, full and empty rhombuses, full and empty upward pointing triangles, and full and empty downward pointing triangles, respectively), for **trans**. (b) Thermal dependence of the imaginary part of ac molar susceptibility χ'' at 110 Hz under the same ac fields.

The pinning of the domain walls is also demonstrated in Figure 12, where the thermal variations of χ' and χ'', plotted for several values of the ac driving field H_{ac}, are compared to the ZFC magnetization measurement. Both components of the ac susceptibility grow when the oscillating field increases, a feature that is typical of ferromagnets.[69,74] At

(71) Tsurkan, V.; Hemberger, J.; Klemm, M.; Klimm, S.; Loidl, A.; Horn, S.; Tidecks, R. *J. Appl. Phys.* **2001**, *90*, 4639.
(72) Levin, E. M.; Pecharsky, V. K.; Gschneider, K. A., Jr. *J. Appl. Phys.* **2001**, *90*, 6255.
(73) Mydosh, J. A. *Spin Glasses: An Experimental Introduction*; Taylor & Francis: London, 1993; p 64.
(74) Balanda, M.; Korzeniak, T.; Pelka, R.; Podgajny, R.; Rams, M.; Sieklucka, B.; Wasiutyński, T. *Solid State Sci.* **2005**, *7*, 1113.

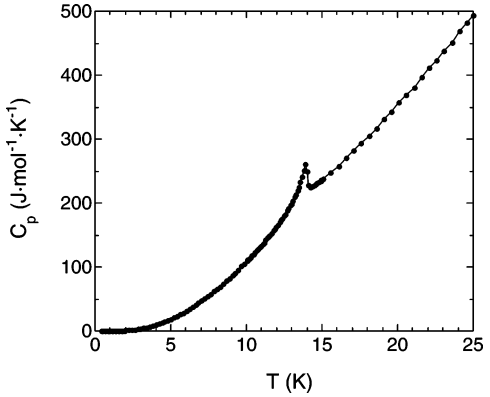

Figure 13. Temperature dependence of the heat capacity of **trans**.

low ac fields (H_{ac} = 0.025 Oe), χ' decreases sharply and continuously upon cooling from T_C. As the driving field increases, the critical point at T_i = 9.5 K appears and becomes more pronounced, and the feature associated with domain wall movement resembles that of the ZFC experiment. Also, the maximum of χ'' shifts toward lower temperatures with increasing driving fields: for higher ac fields, the domain walls are more responsive and the pinning occurs at lower temperatures.

Heat capacity measurements (Figure 13) show the presence of a lambda peak at T_c = 13.9 K. These data prove unambiguously a magnetic phase transition. The absence of any anomaly below the critical temperature indicates that there is no other phase in low-field conditions.

Discussion. The thermomagnetic irreversibility that has been observed in the dc measurements and the complex behavior of the ac susceptibility are often attributed to the presence of a spin glass.[75] However, it is difficult to distinguish in some cases between a spin glass and a ferromagnet with a temperature-dependent coercivity. The picture is further complicated by the fact that glassiness may develop from a magnetically ordered phase, a phenomenon termed reentrance.[75,76] In our case, it means that, even if a second-order phase transition to a ferromagnetic state is clearly established from heat capacity and magnetization measurements, a glassy behavior cannot be discarded. A thorough analysis of the real and imaginary parts of the ac susceptibility as a function of the frequency and strength of the driving field has been proposed as a tool to differentiate between these distinct magnetic behaviors.[71] The general argument is that in spin glasses the driving field interacts with the randomly oriented individual moments (microscopic level), whereas in ferromagnets the magnetic response originates from the interaction with magnetic domains (macroscopic level). For the latter case, a strong correlation between the behavior of the ac susceptibility and the parameters of the domain structure (remanent magnetization and coercive field) should be observed. The significant augmentation in coercivity and thermoremanent magnetization of **trans** that have been detected below 4 K occur in parallel with a maximum of the imaginary component χ'' of the ac susceptibility measured at low frequencies. Further, this maximum is frequency-dependent and follows an Arrhenius-type law, indicating that the slow dynamics of the magnetization results from the energy barrier for movement of the domain walls. As we have seen, the maximum is also dependent on the ac driving field. In higher ac fields, the domain walls are more responsive: the χ'' signal becomes more pronounced and its maximum shifts to lower temperatures. Preliminary measurements of the ac susceptibility of **trans** in a bias dc magnetic field have been previously reported.[49] The presence of the dc field decreases both the in-phase and out-of-phase components and also splits the χ' peak below the critical temperature. These features have been recently attributed to different contributions of the domain wall movement in ferromagnets.[72,77] Additional experiments of this kind using single crystals are underway.

The thermomagnetic irreversibility, evidenced by the difference between the FC and ZFC magnetizations, is also explained by the blocking of the domain walls, which is related to the relative magnitude of the applied (H_A) and coercive (H_C) fields.[69] For $H_A \ll H_C$, M_{ZFC} (and also χ') measurements exhibit a marked decrease in the temperature region where the coercive field increases. For $H_A \gg H_C$, M_{ZFC} and M_{FC} curves tend to merge in a continuous decrease as the temperature rises. The irreversibility is a consequence of the large magnetocrystalline anisotropy of the material. In FC conditions, the magnetization is determined by the net orientation of the spins aligned in the magnetic field. After cooling the sample in zero field, the spins are locked in random directions as a result of the high anisotropy, and their energy may not be enough to overcome the activation barrier, leading to lower values of M_{ZFC}.

Magnetic Properties of cis. Magnetic susceptibility of a polycrystalline sample of **cis** was measured between 2 and 300 K. At room temperature the χT product equals 4.8 emu·K·mol^{-1}, in good agreement with the expected value of 4.8 emu·K·mol^{-1} for three isolated Ni^{2+} ($S = 1$; $g = 2.15$) and two low-spin Fe^{3+} ($S = 1/2$; $g = 2.7$) centers. χT remains almost constant until 20 K. Below this temperature it increases abruptly, reaches a maximum of 186.6 emu·K·mol^{-1}, and falls down upon further cooling. The fit of the reciprocal susceptibility to the Curie−Weiss law in the 50−300 K range (Figure 14, inset) yields constants C = 4.6 emu·K·mol^{-1} and θ = 15.6 K. The positive Curie−Weiss temperature indicates ferromagnetic interactions between adjacent Ni^{2+} and Fe^{3+} ions. In fact, susceptibility increases steeply below 15 K and saturates to a value of 24.3 emu·mol^{-1} (Figure 14), showing a transition to a long-range ferromagnetic order.

The field dependence of the isothermal magnetization (Supporting Information) was measured in the 0−5 T range. At 2 K the first magnetization curve exhibits a rapid increase to a value of 4.60 μ_B at 1 kOe. Then M rises gradually and continuously with the field. At 5 T magnetization equals 7.0 μ_B, far from but pointing to the expected magnetization of saturation per formula (M_{sat} = 9.15 μ_B). The compound has a magnetic hysteresis characterized by a remanent magnetization M_{rem} = 4.74 emu·mol^{-1} and a coercive field H_c = 398 Oe. **cis** is thus a ferromagnet, but its behavior is somewhat softer than that of **trans**.

(75) Wynn, C. M.; Gîrţu, M. A.; Zhang, J.; Miller, J. S.; Epstein, A. J. *Phys. Rev. B* **1998**, *58*, 8508.
(76) Jonason, K.; Mattsson, J.; Nordblad, P. *Phys. Rev. B* **1996**, *53*, 6507.
(77) Becerra, C. C.; Paduan-Filho, A. *Solid State Commun.* **2003**, *125*, 99.

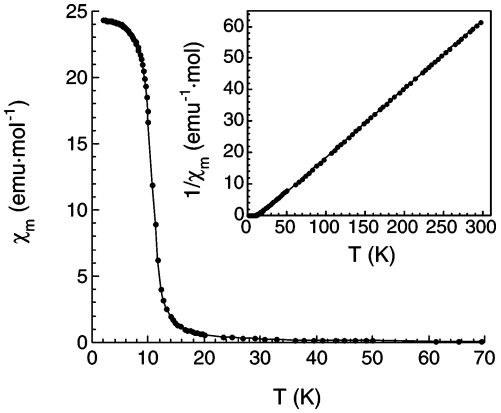

Figure 14. Thermal variation of the molar susceptibility of **cis** in a dc field of 1000 Oe. Inset: Temperature dependence of the inverse molar susceptibility. The straight line corresponds to the fit to the Curie−Weiss law in the 50−300 K range.

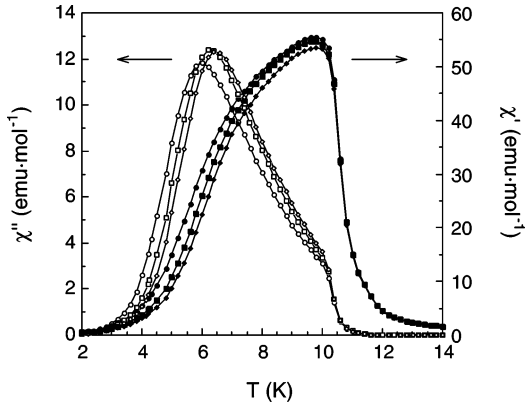

Figure 15. Temperature dependence of the ac molar susceptibility of **cis** (χ', full symbols; χ'', empty symbols) measured in a 3.9 Oe ac field oscillating at frequencies of 10, 110, and 332 Hz (circles, squares, and rhombuses, respectively).

The ordered phase was characterized in the 2−14 K range by ac measurements performed under an ac field of 3.9 Oe oscillating at different frequencies (Figure 15). The real part χ' increases sharply below 12 K, reaches a maximum at 9.8 K, and decays at lower temperatures, describing a shoulder. At the Curie temperature $T_C = 11.0$ K the imaginary part χ'' appears, confirming the onset of a ferromagnetically ordered state. This signal exhibits a frequency-dependent maximum. T_{max} is shifted from 6.0 K at an ac field frequency of 10 Hz to 6.5 K when the ac field oscillates at 332 Hz. Actually, both χ' and χ'' move toward higher temperatures upon increasing the field frequency. The distinctive features of these ac measurements were also observed—amplified, in fact—in **trans**. The frequency-dependent maximum in χ'', which is connected to the shoulder in χ', could therefore be ascribed to a slow dynamics of the magnetic domains in the ordered phase.

Finally, heat capacity measurements were performed in the absence of a dc field (Figure 16). The appearance of a lambda peak with a maximum at $T_C = 10.9$ K unambiguously confirms the existence of a long-range magnetic order. The larger width of the transition peak as compared to **trans** is consistent with the fact that, in the present case, measurements have been performed on less crystalline powders obtained by fast precipitation.

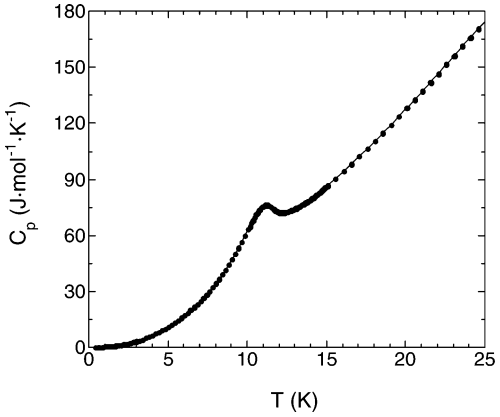

Figure 16. Temperature dependence of the heat capacity of a polycrystalline sample of **cis**.

General Discussion. The magnetic interactions in cyano-bridged metal complexes are well-understood.[78] In the compounds studied herein, they are expected to be ferromagnetic due to the strict orthogonality of t_{2g} (Fe^{3+}) and e_g (Ni^{2+}) orbitals. This is confirmed by the positive θ value observed in the paramagnetic region, despite the fact that cyanide bridges deviate considerably from linearity with bonding angles Ni−N−C in the range between 150.3 and 121.2°. The ferromagnetic exchange interactions propagate throughout the bimetallic layer and give rise to magnetic order. The magnetic ordered phase at the vicinity of T_C is probably a 2D Ising ferromagnet, as pointed out by the presence of a high magnetic anisotropy and the value of the critical exponent β in these layered systems. The bimetallic layers may couple at lower temperatures by very weak interlayer interactions. In most of the cyanide-bridged 2D compounds reported to date, these interactions are negative and an antiferromagnetic ground state results. The weak interlayer exchange interactions can be easily overcome under application of a magnetic field: these compounds are normally metamagnets with a low critical field.[19] In the present case, the interlayer interactions are either negligible or weakly ferromagnetic (the larger interlayer distance of **trans** and **cis** as compared to previously reported compounds may stabilize a ferromagnetic dipolar coupling between layers).[79] In any case, it seems that the slow dynamics of the magnetization in these compounds is associated with both their 2D nature and their uniaxial anisotropy. Below the critical temperature, 2D domains that reproduce approximately the structure of the crystal lattice may form. The domain walls are large and move easily in the bimetallic plane, where significant exchange interactions are present. Out of this plane, however, only very weak interactions exist and the domain walls should be very narrow. Further, this interlamellar space can accumulate structural defects. These two facts hinder the movement of the domain walls in this dimension. This can be the basis of the thermomagnetic irreversibility and slow dynamics in our compounds. The question that arises is about the influence of chirality in this behavior. In principle, the symmetry of the magnetic structure

(78) Verdaguer, M. *Polyhedron* **2001**, *20*, 1115.
(79) Drillon, M.; Panissod, P. *J. Magn. Magn. Mater.* **1998**, *188*, 93.

should be equal to or lower than the symmetry of the nuclear structure and then chiral. However, because the stereogenic centers are located far from the spin carriers, this influence, if present, should be very small. Neutron diffraction experiments should be carried out to confirm this point. Further investigations on these *single-layer magnets*, including magnetic anisotropy measurements and field-dependent specific heat studies, are currently in progress. The present work illustrates how structural and magnetic dimensionalities can be modulated at will to give rise to interesting and peculiar magnetic properties.

Acknowledgment. We thank José M. Martínez-Agudo for his help in the magnetic measurements. This work was supported by the European Commission under Contract No. FP6-515767-2 (MagMaNet NoE). Financial support from the MEC (Spain) (Contract No. MAT2004-03849) and Generalitat Valenciana is also acknowledged.

Supporting Information Available: Thermal variation of the χT product for **trans** and first magnetization curve and magnetic hysteresis at 2 K for **cis** (PDF). This material is available free of charge via the Internet at http://pubs.acs.org.

CM0600879